Motile cilia mediated flow improves sensitivity

and temporal resolution of olfactory computations

Ingrid Reiten 1, Fazil Emre Uslu 2, Stephanie Fore 1, Robbrecht Pelgrims 1, Christa Ringers 1, Carmen Diaz Verdugo 1, Maximillian Hoffman 1, Pradeep Lal 1, Koichi Kawakami 3, Kerem Pekkan 2, Emre Yaksi 1#, Nathalie Jurisch-Yaksi 1#,§

1 Kavli Institute for Systems Neuroscience, Center for Neural Computation, The Faculty of Medicine, NTNU, Olav Kyrres gate 9, 7030 Trondheim, Norway

2 Mechanical Engineering Department, Koc University, Rumelifeneri Yolu, 34450 Istanbul, Turkey

3 Division of Molecular and Developmental Biology, National Institute of Genetics, and Department of Genetics, SOKENDAI (The Graduate University for Advanced Studies), 1111 Yata, Mishima, Shizuoka 411-8540, Japan

Corresponding authors

§ Lead author

Correspondance to

nathalie.jurisch-yaksi@ntnu.no, Kavli Institute / CNC, The Faculty of Medicine, NTNU, Olav Kyrres gate 9, Postboks 8905, 7030 Trondheim, Norway, Tel +47 (735) 98276

emre.yaksi@ntnu.no, Kavli Institute / CNC, The Faculty of Medicine, NTNU, Olav Kyrres gate 9, Postboks 8905, 7030 Trondheim, Norway, Tel +47 (735) 98276

Summary

Motile cilia are actively beating hair-like structures that cover the surface of multiple epithelia. The flow that ciliary beating generates is utilized for diverse functions and depends on the spatial location and biophysical properties of cilia. Here, we showed that the motile cilia in the nose of aquatic vertebrates are spatially organized and stably beat with an asymmetric pattern, resulting in a robust and stereotypical flow around the nose. Our results demonstrate that these flow fields attract odors to the nose pit and facilitate detection of odors by the olfactory system in stagnant environments. Moreover, we showed that ciliary beating quickly exchanges the content of the nose, thereby improving the temporal resolution of the olfactory system for detecting dynamic changes of odor plumes in turbulent environments. Altogether, our work unravels a central function of ciliary beating for generating flow fields that increase the sensitivity and the temporal resolution of olfactory computations in the vertebrate brain.

Keywords

Cilia, motile cilia, multiciliated cells, olfactory system, olfactory coding, fluid dynamics, flow fields, zebrafish, salmon

Introduction

Cilia are microscopic hair like structures extending from the surface of almost all cells of the vertebrate body [1]. Motile cilia actively move and drive directional flow patterns across tissues, whereas primary cilia are enriched in receptors and play crucial sensory roles [2]. It is therefore not surprising that mutations affecting the structure, function or presence of cilia result in multiple human pathologies, collectively known as ciliopathies [3]. Throughout vertebrate evolution, the directional flow generated by the beating of motile cilia was utilized for diverse set of functions [4]. For example, in brain ventricles, cilia-mediated flow allows the delivery of nutrients and signaling molecules as well as the clearance of waste products, such as neurotoxins and molecular aggregates [5, 6]. Whereas in the respiratory tract motile cilia control the thickness of the protective mucus and clearance of toxic substances [7-9]. Despite the clear role of cilia mediated flow in all these vital processes, we still know very little about how coordinated ciliary beating generates complex hydrodynamic flow fields and what other important biological functions are mediated by this flow [4].

One of the main obstacles hampering the studies of motile cilia function is the difficulty of monitoring ciliary beating patterns and flow fields simultaneously, in living organisms. Here we introduce a new model for ciliary beating, the motile cilia of the nose, which thanks to their accessibility facilitate in depth studies of motile ciliary function in vertebrates. The nasal epithelium is one of the most accessible tissues decorated with motile cilia, where they move liquid or mucus in the nasal cavity [10, 11]. While the presence of mucus is important for dissolving odors and shuttling them to olfactory receptor neurons (ORNs) [12], it is unclear whether the motile cilia of the nose have a more direct sensory function and can facilitate the detection of odors or modulate olfactory computations by generating flow fields. In this study, by taking advantage of the accessible olfactory epithelium of zebrafish larvae, we characterized how ciliary beating generates robust stereotypical flow, regulates odor sampling and improves temporal resolution of olfactory computations in the brain.

Results

Multiciliated cells in the nose pit are spatially organized and beat their cilia at a distinct frequency

In 4 days old zebrafish larvae, the nose pits are hollow cup-like structures located in the snout (Fig 1A,A'). Multiple cell types constitute the olfactory epithelium (Fig 1A'') and can be differentiated according to their morphology[13]. Multiciliated cells (MCCs) are cuboidal cells, which harbor large bundles of acetyl tubulin positive motile cilia (Fig 1A'-A'''). They are arranged in a layer surrounding the rim of the nose pit (Fig S1). In contrast, the ciliated ORNs have primary cilia with sensory function and are characterized by a pear shaped body [14]. ORNs are located below the MCCs at the bottom of the pit and exhibit dendritic knobs bearing fewer non motile cilia decorated with the olfactory receptors (Fig 1A'', A''', Fig S1). We observed that the ciliary beating of MCCs interferes with the transmission of light and can readily be measured as periodic oscillations of pixel intensity by using a standard microscope at relatively high spatial and temporal (>100Hz) resolution (Movie S1). In order to quantify the spatial distribution of the ciliary beating frequency (CBF) we performed Fourier transform in every image pixel across 10 seconds and visualized the peak frequency as a heat map (Fig 1B, C). Regions with robust CBF overlap with the area where motile cilia extend into the cavity of the nose pit. No CBF was detected in the middle or outside the pit (Fig 1B). The average CBFs of a total of 130 larvae show a normal distribution ranging from 18.9 to 29.5 Hz with a mean value of 24.4 +/- 2.35 Hz (Fig 1C-D). Interestingly distinct patches with robust local peak beating frequencies can be distinguished and remain stable over time (Fig 1B,E).

Motile cilia beat with an asymmetric stroke and generate stereotypical flow fields around the nose

In order to further characterize the precise beating pattern, velocity and direction of motile cilia, we identified an enhancer trap line, that sparsely labels MCCs in the nose pit by green fluorescent protein (*hspGGFF19B;UAS:GFP*). Light sheet microscopy recordings with high spatial and temporal resolution (900Hz) showed that motile cilia beat in an asymmetric manner (Movie S2 and Fig 2A and 2B). This asymmetric beating is composed of a fast effective stroke and a slow recovery stroke, which is in line with other studies on motile cilia of MCCs [4]. We observed that during the effective stroke, individual cilia extend fully with a maximal velocity of 1.9 +/- 0.3mm/s (total of 9 cells from 4 larvae). Later, during the slow recovery stroke, they retract by 180 degrees and stay as a bundle close to the cell body, creating a whip-like motion (Fig 2A). This high resolution measurement showed that the complete ciliary stroke for an individual MCC

lasts 38.5 +/- 3.7 ms which corresponds to the mean frequency of 26.2 +/- 2.5 Hz and is in line with the mean CBF obtained by transmission light microscopy (Fig 1D).

Previous studies suggest that the asymmetric beating of motile cilia is important for generating complex flow patterns in brain ventricles [6] and in the mucosa of multiple tissues [4]. In order to visualize the flow generated by ciliary beating in zebrafish nose pit we imaged the flow fields from a dorsal view using fluorescent particles and confocal microscopy. We quantified the flow fields by using particle image velocimetry (PIV), an analytical method that is widely used in the field of biological fluid mechanics [15-18]. PIV measurements revealed that ciliary beating generates a fast and stereotypical flow around the snout that draws water medially from the heading direction of the larvae and ejects laterally towards both sides (Fig 2C, Movie S3). We observed that these microscopic jet turbines, powered by the motile cilia of only 8.7+/-2.2 μm in size, can attract water to the nose pits from more than 200 μm (Fig 2C) and create a persistent convection zone. Measurements around the nose pits with faster time resolution revealed that the maximal flow velocities can go up to 120μm/s (mean is 98+/-32 μm/s) and are not significantly different at the inlet and the outlet of the olfactory pit (Fig 2D, F). We used these flow velocities to estimate the residence time of an odor particle near the olfactory epithelium through the pit. Our calculation showed that the fluid content of the nose pit is fully exchanged within 0.41+/-0.09 sec due to the coordinated action of ciliary beating (Fig 2G). These flow fields are in line with the arrangement of asymmetric beating from multiple individual MCCs around the nose pit obtained by light sheet microscopy, where MCCs located medially beats laterally toward the nose pit, and cells located laterally beats outwards toward the eye (summarized in model Fig 2E). We also measured the flow fields at different depths along the medial-lateral axis. Our measurements revealed that the flow fields draw water from all directions at the medial positions of the snout (Fig 2H), and eject water dorsally at the lateral part of the snout (Fig 2I). Altogether, our analysis revealed that even though the nose pit is a rather homogenous cup at 4 days, the location and beating pattern of motile cilia allow already a medio-lateral and anterio-posterior current flow, as observed in the adult nose pits of some fish species [19, 20].

Next, we set to verify the causal relationship between ciliary beating and the flow fields around the nose by using a zebrafish mutant line (*schmalhans, smh*) that displays ciliary motility defects in motile cilia of various tissues [21]. Importantly, this specific mutation was shown to retain the

general structure and length of both primary and motile cilia, albeit the stasis in motile cilia [21]. In line with these findings, our acetyl-tubulin staining confirmed the presence of cilia in the nose pit of *smh-/-* homozygous mutant (Fig 3A, A'). Moreover we observed a complete paralysis of motile cilia in our transmission microscopy measurements in the nose (Fig 3B, B'). Consequently, the stasis in motile cilia of *smh-/-* zebrafish resulted in a loss of the flow fields around the nose pits and the snout (Fig 3C, C', Movie S4) in PIV measurements. Altogether, these results demonstrate a direct role of motile ciliary beating in the generation of the flow fields around the nose.

Motile cilia in the nose are conserved across most vertebrates from fish to rodents [11, 13, 19, 20, 22, 23]. To characterize ciliary beating and motile-cilia driven flow in the nose of other teleost fish species, we performed similar experiments in salmon larvae. The olfactory pits of salmon larvae at 4 days post hatching are located at the snout (Fig S2A) and consist of a channel with one anterior and one posterior opening (Fig S2B). Our acetyl-tubulin staining in salmon larvae revealed positively labelled cilia in various locations around the nose, with an enrichment at the posterior opening (Fig S2B). Next we observed that cilia at the posterior opening are motile and beat at an average frequency of 26.5+/-2.0 Hz (Fig S2C and S2D), in line with the values obtained in zebrafish. Finally, PIV measurements revealed a strong anterio-posterior current through the nose (Fig S2E, F). Altogether, our results revealed that the motile cilia in the nose of several aquatic vertebrates have similar beating properties and generate robust and stereotyped flow fields around the nose even at larval stages, which indicates an important function for this highly conserved phenomenon.

Lack of ciliary beating hampers attraction of odors to nose pit and neural responses to odors in stagnant environments

The overall shape and direction of the flow fields around the nose pits suggests that the motile cilia of the nose may attract odors to the olfactory pit. We hypothesized that this phenomenon can facilitate detection of odors especially in stagnant aquatic environments, for example a zebrafish larvae at rest in a pond. In order to test this hypothesis, we delivered a fluorescently labelled odor using a pressure injector and we simultaneously measured the odor dynamics and the odor evoked neural responses using two-photon microscopy, in zebrafish expressing calcium indicator

GCamp6s panneuronally (*HuC:Gcamp6s*) [24]. Our results confirmed that flow fields generated by the beating of motile cilia can attract odors from over 200µm away from the nose pit (Fig 3D, E, Movie S5 top). Moreover, we observed that these flow fields facilitate odor detection and elicit odor responses at ORNs and at the first relay of odor information in the brain, the olfactory bulb (OB). On the contrary, *smh-/-* zebrafish failed to attract odors to the nose and showed no detectable odor responses in ORNs or in OB (Fig 3D', E', Movie S5 bottom). Given enough time, very low concentrations of odors may still passively diffuse to the nose pit of *smh-/-* due to Brownian motion [25], but such low concentrations were not able to elicit odor responses (Fig 3E'). Altogether, our data shows that the motile ciliary beating generates flow and attracts odors to the nose pit facilitating odor detection especially in stagnant aquatic environments, when the fish is at rest.

Lack of ciliary beating does not affect the odor selectivity of olfactory receptor neurons under constant flow

Zebrafish larvae are not continuously at rest nor the aquatic environments are always still. In order to test how *smh-/-* zebrafish with impaired ciliary beating and absent flow fields will respond to odors in aquatic environments with flow, we used a tubing system that constantly perfuses the animals' nose. When odors were delivered for 20 seconds under constant flow, our calcium imaging results showed that the ORNs of the *smh-/-* zebrafish respond to odors with slower kinetics than controls (Fig 4A,B). However, in these conditions, we observed no significant difference in the ratio of responding ORNs (Fig 4C) or in the odor selectivity of responding ORNs for 3 different categories of odors (Fig 4D) between *smh-/-* and control larvae. We also saw no significant difference in the olfactory coding efficiency in *smh-/-* and control larvae, measured by correlations of multi neuronal activity patterns in response to different categories of odors (Fig 4E, F). Altogether, our results showed that, when odors are presented under constant flow and for prolonged periods of time, odor coding of ORNs is not affected in *smh-/-* zebrafish with impaired ciliary beating. Hence, neurophysiological properties of ORNs for olfactory computations are not affected by the *smh* mutation.

Ciliary beating increases the temporal resolution of the olfactory system and enhances the detection of fast changes in odor plumes.

In nature, odor plumes are rather dynamic and foraging animals experience odor plumes temporarily and with short inter stimulus intervals [26-29]. We expect that wildtype zebrafish with active flow around the snout would attract odors and eject them from the nose, rapidly updating the content of the nose pit. Such a mechanism would in principle increase the temporal resolution of the olfactory computations in the brain. Whereas, a system that relies on passive diffusion of odors, such as *smh-/-* nose pits would have difficulties to detect fast changing odor plumes and thus reduce the temporal resolution of the neuronal computations. In order to test this hypothesis, we systematically varied the temporal aspects of the odor input (Fig 5A) and compare the performance of *smh-/-* and control ORNs and OB neurons in encoding the temporal dynamics of fluctuating odors by using two-photon microscopy and calcium imaging (Movie S6). We first tested how a short (0.5 second) odor pulse in a constant flow (2ml/min) is encoded at the level of ORNs and the OB (Fig5 B, C, Video S6). In line with our results of Fig 4B, odor stimuli that are delivered by the exact same input dynamics at the source (Fig 5C) displayed slower dynamics in *smh-/-* zebrafish (Fig 5C'-C'''). Odor delivery or responses took a significantly longer time to reach the maximum at the nose pit (Fig 5C'), ORNs (Fig 5C'') and OB (Fig 5C''') in *smh-/-* zebrafish (Fig 5D). Moreover, the odor dwell time, calculated as the duration of odor stimuli in the olfactory pit from the time odors arrive and leave the pit, was significantly larger in *smh-/-* larvae compared to controls (Fig 5E), highlighting the importance of ciliary beating in reducing the residence time of odors in the nose pit.

Next, we tested the performance of *smh-/-* and wildtype zebrafish in encoding temporally dynamic odor stimuli, by systematically varying the inter-stimulus intervals between odor pulses gradually decreasing from 8 to 4 and 2 seconds (Fig 5A, Movie S7). We quantified and compared the temporal resolution of the olfactory computations by using two different measures: 1) the power spectral density (PSD) of the odor induced fluctuations at the frequency of stimulus delivery and 2) the average amplitude of the odor induced oscillations normalized to the maximum response. These measures were calculated from fluorescent odor signals at the input and the nose pit as well as the calcium signals of neuronal activity of the ORNs and the OB (Fig 5B). Our measurements showed that fluctuating odor stimuli with decreasing inter stimulus intervals are sampled significantly faster and with higher temporal resolution at the nose pits of controls compared to *smh-/-* larvae (Fig 5F, F', G, H, I, I', J, K, L, L', M, N). In line with these findings, we observed that odor fluctuations are encoded significantly better at the level of the

olfactory bulbs at all interstimulus intervals by control animals (Fig 5F’’’, I’’’, L’’’). In fact, increasing the difficulty of the task by challenging the animals with faster odor fluctuations lead to more significant differences in temporal encoding of odors by the OB neurons of control animals (Fig 5G, H, J, K, M, N). Finally, we observed that the OB is in general better in encoding odor fluctuations than their input neurons, ORNs (Fig 5F’’, G, H, I’’, J, K, L’’, M and N).

Discussion

Altogether, our results showed that detecting odors in stagnant and turbulent environments depends on the fluid dynamics properties of the nose pit. This is particularly important for aquatic vertebrates since their olfactory cavity is often not connected to respiration and the passive diffusion of odorant molecules in water is slow. In aquatic animals, odors can be driven into the nose by various mechanisms [22, 23]. For example, differential water pressure between incurrent and excurrent nostrils can result from the forward motion of the fish or incoming flow. As an alternative solution few aquatic vertebrates evolved accessory sacs in their olfactory organs which can be expended and compressed [30]. Lobsters were shown to move their antennules to draw water into the olfactory epithelium [27]. In addition to these potential solutions that are evolved to improve aquatic olfaction, here we demonstrate that motile cilia-driven flow, which was observed in various adult teleosts species[19, 20, 23], is an efficient and fast olfactory sampling method as previously suggested [19]. A similar mechanism may potentially be utilized in the mammalian nose. Our data showed for the first time how the motile cilia decorating the nose pit act as a very powerful water turbine and generate strong and robust flow fields that allow fish to quickly exchange the content of the nose. Importantly, this mechanism increases the sensitivity and temporal resolution of odor computations both in stagnant and running aquatic environments and does not require muscle contraction. Interestingly in hagfish and lampreys, which are considered evolutionary primitive fish species, the respiratory flow initiated by the velum contraction passes through the olfactory chamber toward the gills and thus draw odors [31]. Thus, from an evolutionary perspective, it appears that cilia driven flow in the nose pit is rather novel and may underlie a powerful and energy efficient mechanism to draw odors in the nose. Altogether, we propose that this mechanism might have evolved to facilitate better sampling of dynamically changing odor plumes and thereby enhancing the temporal resolution of olfactory computations. It is an intriguing correlation that the motile cilia in the nose of most

vertebrates and in the airways of mammals generate ciliary beating with similar principles, highlighting a possible evolutionary relationship between these structures.

Thanks to the optical accessibility of zebrafish nose pit, we could fully characterize how motile cilia beat to generate a robust flow in an intact organism. First, the asymmetric beating pattern that we show for the motile cilia of the nose is conserved across many MCCs located along the brain ventricles, spinal cord and respiratory tract [4]. Second, the average CBF of zebrafish and salmon olfactory MCCs is rather uniform across individuals and lies between 20 and 30Hz. In contrast, big variations in CBF from 10 to 40Hz were reported for epithelia depending on the specimen preparation in past studies. Third, we showed that flow characteristics resulting from the specific location and asymmetric beating of motile cilia are tailored to the organ's need. In the brain ventricles, beating cilia can concentrate molecules locally or prevent entry to another ventricular area by generating boundaries [6]. Our findings suggest here that the robust and directional flow, generated by motile cilia in the nose pit, guarantees an efficient exposure of ORNs to odors but for a restricted time. Even though it is now clear that fluid dynamics are regulated by the power and directionality of ciliary beating, the cellular and molecular mechanisms underlying the establishment of asymmetric ciliary beating remain to be fully understood. Altogether, having such a conserved ciliary function outside the body of a living vertebrate provides a plethora of methods to image and interfere with ciliary function, and thus could serve as model to better understand the chemical, physical and genetic factors regulating ciliary beating.

Experimental procedures

Please see the Supplemental Information for details of the methods

Author contributions

IR, SF, CR, NJY performed experiments. FEU quantified flow parameters under the supervision of KP. RP designed the hardware and wrote the software for image acquisition by transmission microscopy. MH built the light-sheet microscope. CDV wrote MATLAB codes for aligning two-photon data and detecting cells. KK constructed the *hspGGFF19B* enhancer trap line. PL characterized the *hspGGFF19B* enhancer trap line. NJY and EY conceived the study, designed the project and wrote the manuscript.

Acknowledgments

We would like to thank I Drummond (Massachusetts General Hospital) for the *smh* mutant line and critical reading of the manuscript, X Lin (Mayo Clinic) for the *Foxja:GFP* plasmid, M Ahrens (Janelia farm) for the *HuC:GCamp6* transgenic line, the design of the lightsheet microscope and its software Zebrascope, C Brandt for injecting the *Foxj1a:GFP* construct in zebrafish embryos and M. Andresen for managing the zebrafish facility and for genotyping. We would like to thank Aquagen AS for providing us with salmon larvae. This work was funded by the ERC starting grants 335561 (EY) and 307460 (KP) as well as the EMBO-IG program (KP). Work in the EY lab is funded by the Kavli Institute for Systems Neuroscience at NTNU, Trondheim, Norway.

.

References

1. Fliegauf, M., Benzing, T., and Omran, H. (2007). When cilia go bad: cilia defects and ciliopathies. Nat Rev Mol Cell Biol *8*, 880-893.
2. Berbari, N.F., O'Connor, A.K., Haycraft, C.J., and Yoder, B.K. (2009). The primary cilium as a complex signaling center. Current biology : CB *19*, R526-535.
3. Hildebrandt, F., Benzing, T., and Katsanis, N. (2011). Ciliopathies. The New England journal of medicine *364*, 1533-1543.
4. Brooks, E.R., and Wallingford, J.B. (2014). Multiciliated cells. Current biology : CB *24*, R973-982.
5. Veening, J.G., and Barendregt, H.P. (2010). The regulation of brain states by neuroactive substances distributed via the cerebrospinal fluid; a review. Cerebrospinal Fluid Res *7*, 1.
6. Faubel, R., Westendorf, C., Bodenschatz, E., and Eichele, G. (2016). Cilia-based flow network in the brain ventricles. Science *353*, 176-178.
7. Stannard, W., and O'Callaghan, C. (2006). Ciliary function and the role of cilia in clearance. J Aerosol Med *19*, 110-115.
8. Shah, A.S., Ben-Shahar, Y., Moninger, T.O., Kline, J.N., and Welsh, M.J. (2009). Motile cilia of human airway epithelia are chemosensory. Science *325*, 1131-1134.
9. Johanson, C.E., Duncan, J.A., 3rd, Klinge, P.M., Brinker, T., Stopa, E.G., and Silverberg, G.D. (2008). Multiplicity of cerebrospinal fluid functions: New challenges in health and disease. Cerebrospinal Fluid Res *5*, 10.
10. Getchell, T.V., Margolis, F.L., and Getchell, M.L. (1984). Perireceptor and receptor events in vertebrate olfaction. Prog Neurobiol *23*, 317-345.
11. Harkema, J.R., Carey, S.A., and Wagner, J.G. (2006). The nose revisited: a brief review of the comparative structure, function, and toxicologic pathology of the nasal epithelium. Toxicol Pathol *34*, 252-269.
12. Pelosi, P. (2001). The role of perireceptor events in vertebrate olfaction. Cell Mol Life Sci *58*, 503-509.
13. Hansen, A., and Zeiske, E. (1998). The peripheral olfactory organ of the zebrafish, Danio rerio: an ultrastructural study. Chem Senses *23*, 39-48.
14. Kermen, F., Franco, L.M., Wyatt, C., and Yaksi, E. (2013). Neural circuits mediating olfactory-driven behavior in fish. Frontiers in neural circuits *7*, 62.
15. Adrian, R.J. (2005). Twenty years of particle image velocimetry. Exp Fluids *39*, 159-169.
16. Chen, C.Y., Patrick, M.J., Corti, P., Kowalski, W., Roman, B.L., and Pekkan, K. (2011). Analysis of early embryonic great-vessel microcirculation in zebrafish using high-speed confocal muPIV. Biorheology *48*, 305-321.
17. Pekkan, K., Chang, B., Uslu, F., Mani, K., Chen, C.Y., and Holzman, R. (2016). Characterization of zebrafish larvae suction feeding flow using mu PIV and optical coherence tomography. Exp Fluids *57*.
18. Chen, C.Y., Menon, P.G., Kowalski, W., and Pekkan, K. (2013). Time-resolved OCT-mu PIV: a new microscopic PIV technique for noninvasive depth-resolved pulsatile flow profile acquisition (vol 54, 1426, 2013). Exp Fluids *54*.

19. Bashor, D.P., Beuerman, R.W., and Easton, D.M. (1974). Ciliary action and normal movement of odorant wavefronts in garfish nasal capsule ofLepisosteus osseus. Experientia *30*, 777-779.
20. Døving, K.B., Dubois-Dauphin, M., Holley, A., and Jourdan, F. (1977). Functional Anatomy of the Olfactory Organ of Fish and the Ciliary Mechanism of Water Transport. Acta zoologica *58*, 245-255.
21. Panizzi, J.R., Becker-Heck, A., Castleman, V.H., Al-Mutairi, D.A., Liu, Y., Loges, N.T., Pathak, N., Austin-Tse, C., Sheridan, E., Schmidts, M., et al. (2012). CCDC103 mutations cause primary ciliary dyskinesia by disrupting assembly of ciliary dynein arms. Nature genetics *44*, 714-719.
22. Kasumyan, A. (2004). The olfactory system in fish: structure, function, and role in behavior. Journal of Ichthyology *44*, S180.
23. Cox, J.P. (2008). Hydrodynamic aspects of fish olfaction. J R Soc Interface *5*, 575-593.
24. Quirin, S., Vladimirov, N., Yang, C.T., Peterka, D.S., Yuste, R., and Ahrens, M.B. (2016). Calcium imaging of neural circuits with extended depth-of-field light-sheet microscopy. Opt Lett *41*, 855-858.
25. Krynicki K, Green CD, and DW., S. (1978). Pressure and temperature dependence of self-diffusion in water. Faraday Discuss Chem soc *66*, 199-208.
26. Vickers, N.J. (2000). Mechanisms of animal navigation in odor plumes. Biol Bull *198*, 203-212.
27. Koehl, M.A., Koseff, J.R., Crimaldi, J.P., McCay, M.G., Cooper, T., Wiley, M.B., and Moore, P.A. (2001). Lobster sniffing: antennule design and hydrodynamic filtering of information in an odor plume. Science *294*, 1948-1951.
28. Nagel, K.I., Hong, E.J., and Wilson, R.I. (2015). Synaptic and circuit mechanisms promoting broadband transmission of olfactory stimulus dynamics. Nature neuroscience *18*, 56-65.
29. Schulze, A., Gomez-Marin, A., Rajendran, V.G., Lott, G., Musy, M., Ahammad, P., Deogade, A., Sharpe, J., Riedl, J., Jarriault, D., et al. (2015). Dynamical feature extraction at the sensory periphery guides chemotaxis. eLife *4*.
30. Kux, J., Zeiske, E., and Osawa Y. (1988). Laser Doppler velocimetry measurement in the model flow of a fish olfactory organ. Chem Senses *13*, 257-265.
31. Holmes, W.M., Cotton, R., Xuan, V.B., Rygg, A.D., Craven, B.A., Abel, R.L., Slack, R., and Cox, J.P. (2011). Three-dimensional structure of the nasal passageway of a hagfish and its implications for olfaction. Anat Rec (Hoboken) *294*, 1045-1056.

Figures and Figure legends

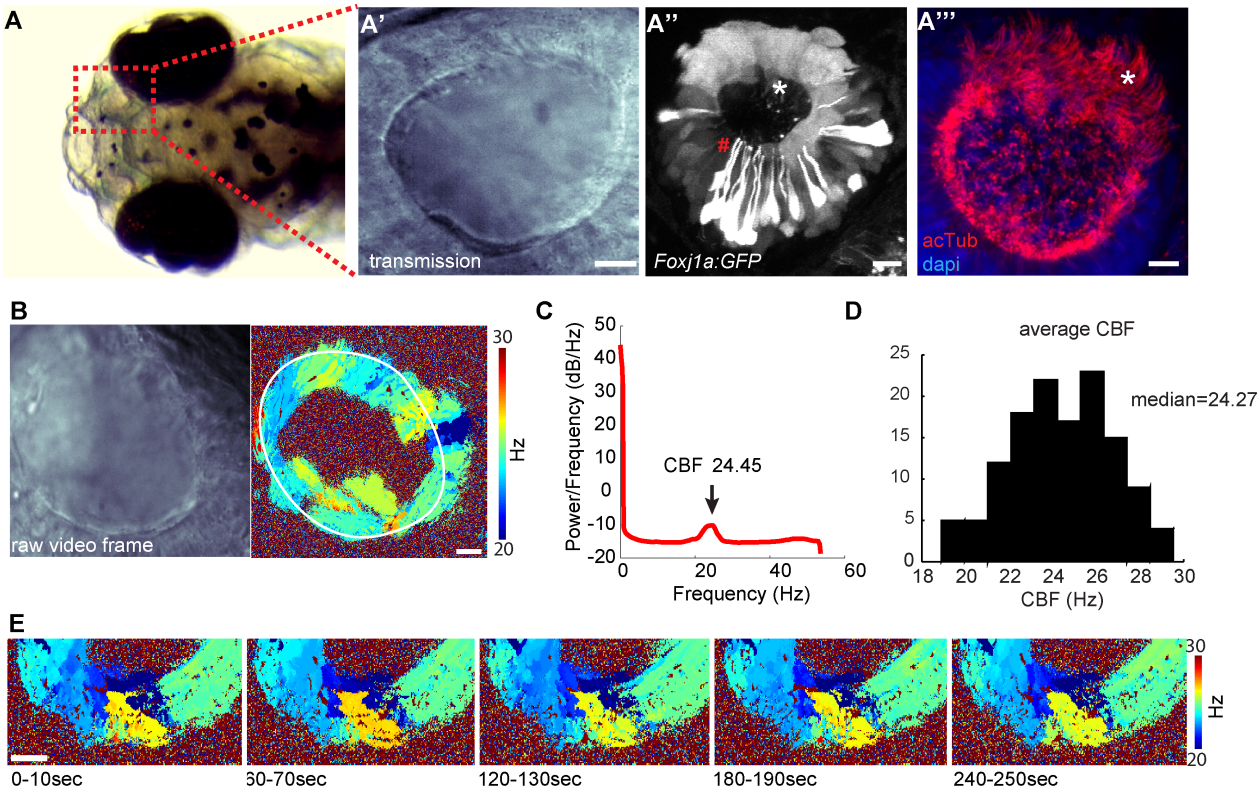

Figure 1: Multiciliated cells in the nose pit of 4 days old zebrafish larvae are spatially organized and beat their cilia at a distinct frequency. (A) Representative image of a 4 days old zebrafish larvae. The nose pit, indicated by the red dashed inlet, appears as a hollow cup in transmission microscopy (A'). (A'') Two photon microscopy image of the nose pit in *Foxj1a:GFP* zebrafish. Cuboidal-shaped multiciliated cell with motile cilia are indicated by "*" and pear-shaped ciliated olfactory receptor neurons are indicated by "#". (A''') Confocal microscopy image of the nose pit, where all cilia are labelled by acetyl tubulin staining (red) and cell nuclei are labelled with DAPI staining (blue). Note longer motile cilia indicated by "*". (B) Fast (100Hz) transmission microscopy recordings in the nose pit of a representative animal (left) showed that the patches of motile cilia beat at frequencies ranging from 20Hz to 30Hz (right, nose cavity is indicated with a white line) , with an average of 24.45 Hz as shown by power spectral density analysis (C). (D) Average ciliary beating frequency from 130 zebrafish larvae range from 19 to 29Hz, with a median of 24.27Hz. (E) Beating frequency is stable during 5 min, reported for one representative pit at 1min intervals. Scale bars are 10µm. See also Figure S1, S2 and Movie S1

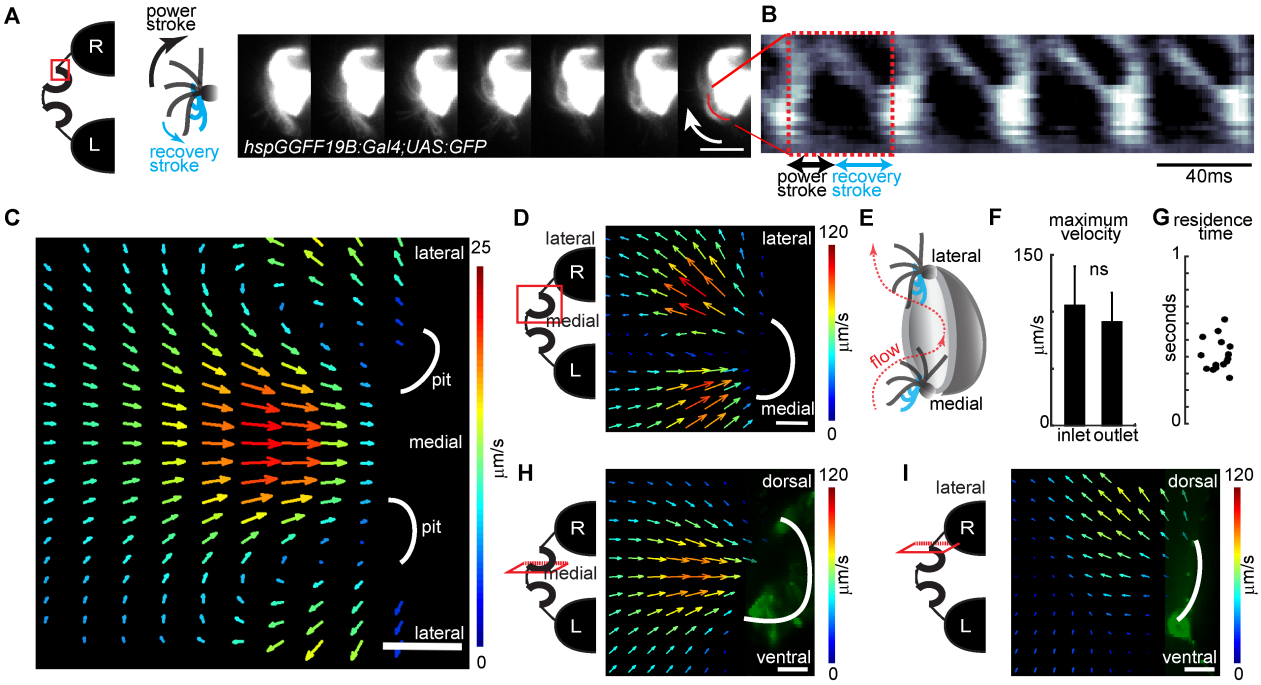

Figure 2: Motile cilia beat with an asymmetric stroke and generate stereotypical flow fields around the nose. (A) Beating pattern of two adjacent multiciliated cells, sparsely labelled with GFP (*hspGGFF19B:Gal4;UAS:GFP*), recorded by light sheet microscopy at 900 Hz. Red inlet on the left scheme marks the region of recording around the nose. Montage representing 7 images separated by 4.5ms on the right. Arrow marks the direction of beating. Note the asymmetric curvature of cilia during strokes as exemplified in the model on the left. (B) Kymogram of pixel intensity along the red line shows an asymmetric beating pattern composed of a fast power stroke and a slow recovery stroke. A complete beating cycle has a period of 40ms. (C) Flow fields are measured by particle image velocimetry using confocal microscopy images (2.15 Hz) of fluorescent particles around the nose pits (indicated by white lines) of 4 days old zebrafish larvae. Imaging plane viewed from dorsal. Warm colors and large arrows indicate strong flow. Direction of the arrows indicate the direction of the flow. Note that the stereotypical flow fields generated by motile cilia attract water from medial regions into the nose pits and ejects it towards the lateral directions. (D) Close up and faster (19.6 Hz) measurements of the dorsally viewed flow fields near the right nose pit. Note high flow rates of inflow (medially) and outflow (laterally) near the nose pits. Red inlet in the scheme on the left depicts the imaged region. (E) Model summarizing the directional orientation of asymmetrically beating motile cilia along the nose pits based on light-sheet microscopy measurements of individual sparsely labelled cilia from 11 animals. Cells located medially beat towards the pit. Cells located laterally beat toward the outside of the pit. (F) Maximal flow velocities at the inlet and outlet of the nose pits are not significantly different (15 nostrils from 7 larvae). Error bars are std. (G) Residence times of particles in the nose pit measured in 15 nostrils from 7 larvae, calculated based on inflow, outflow and the volume of the nose pit. (H-I) Flow fields at the right nose pit laterally viewed at two different depths, medial (H) and lateral (I) as indicated by red inlets in the left scheme. *Foxj1a:GFP* larvae were used (n=4). Note that (H) at medial plane inflow attracts water from all directions, (I) at the lateral plane outflow ejects water mostly dorsally. Scale bars are 10µm (A), 100µm (C) and 20µm (D-I). p-value by signrank test, ns=non significant. See also Figure S2 and Movie S2 and S3

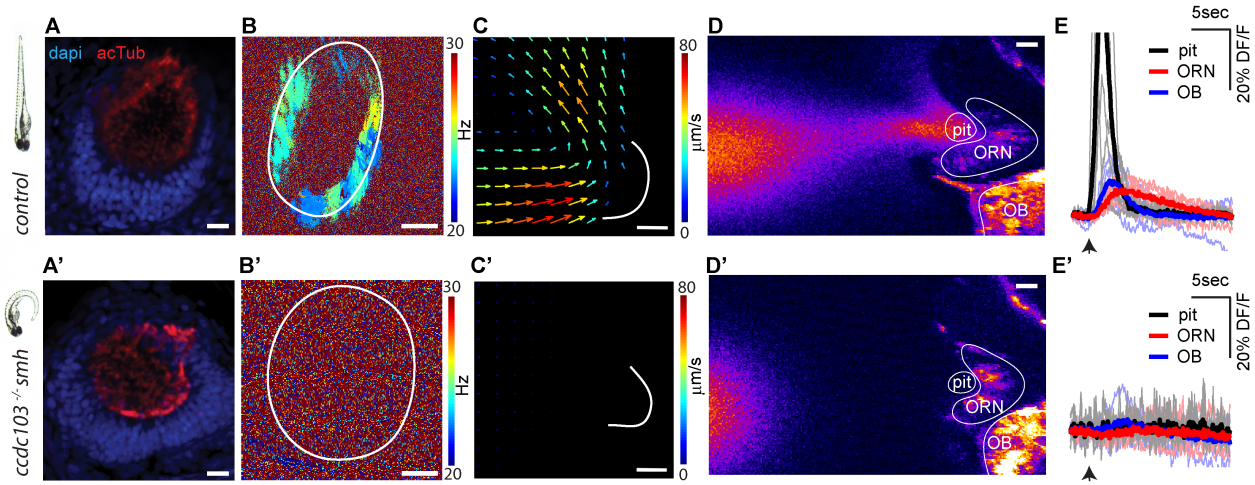

Figure 3: Lack of ciliary beating in the multiciliated cells of *smh-/-* zebrafish diminishes flow fields around the snout, hampers attraction of odors to nose pit and consequently impairs neural responses to odors in stagnant environments. (A-A') *smh-/-* larvae that are identified by their bend body axis (left) have a normal ciliary distribution in the nose pit, confirmed by acetyl tubulin staining. (B-B') No ciliary beating (n=9 for *smh -/-* CBF=none, n=10 control CBF=23.9+/-1.2Hz) and (C-C') no flow fields (n=3 for *smh -/-* and controls) are detected in the nose pit of *smh-/-* larvae, when compared to control animals. (D-E) Fluorescently labelled food odor is released from a capillary using a microinjector and odor flow dynamics and neural responses to odors are imaged using two-photon microscopy in *HuC:GCamp6s* zebrafish expressing transgenic calcium indicators. No external flow is applied. (D,D') Raw video frames following microinjection were averaged. Note that the flow generated by motile cilia can attract odors to the nose pit in control zebrafish (D). Whereas *smh -/-* larvae fail to attract odors (D'). (E-E') Time course of odor dynamics in the nose pit and neural responses to odors in ORN and OB in control (E) and *smh-/-* (E') larvae, represented as percentage change of fluorescence over time (DF/F). Note that in controls the odor is rapidly attracted and ejected from the nose pit (black), which results in transient odor responses in ORNs (red) and OB (blue). In contrast , *smh-/-* larvae do not attract odor to the nose pit and thus ORN and OB do not display calcium activity. Light lines are individual traces, dark lines are average, black arrows mark the time of odor injections. n=7 (wt) & 6 (*smh -/-*). All scale bars are 20µm. See also Movie S4 and S5

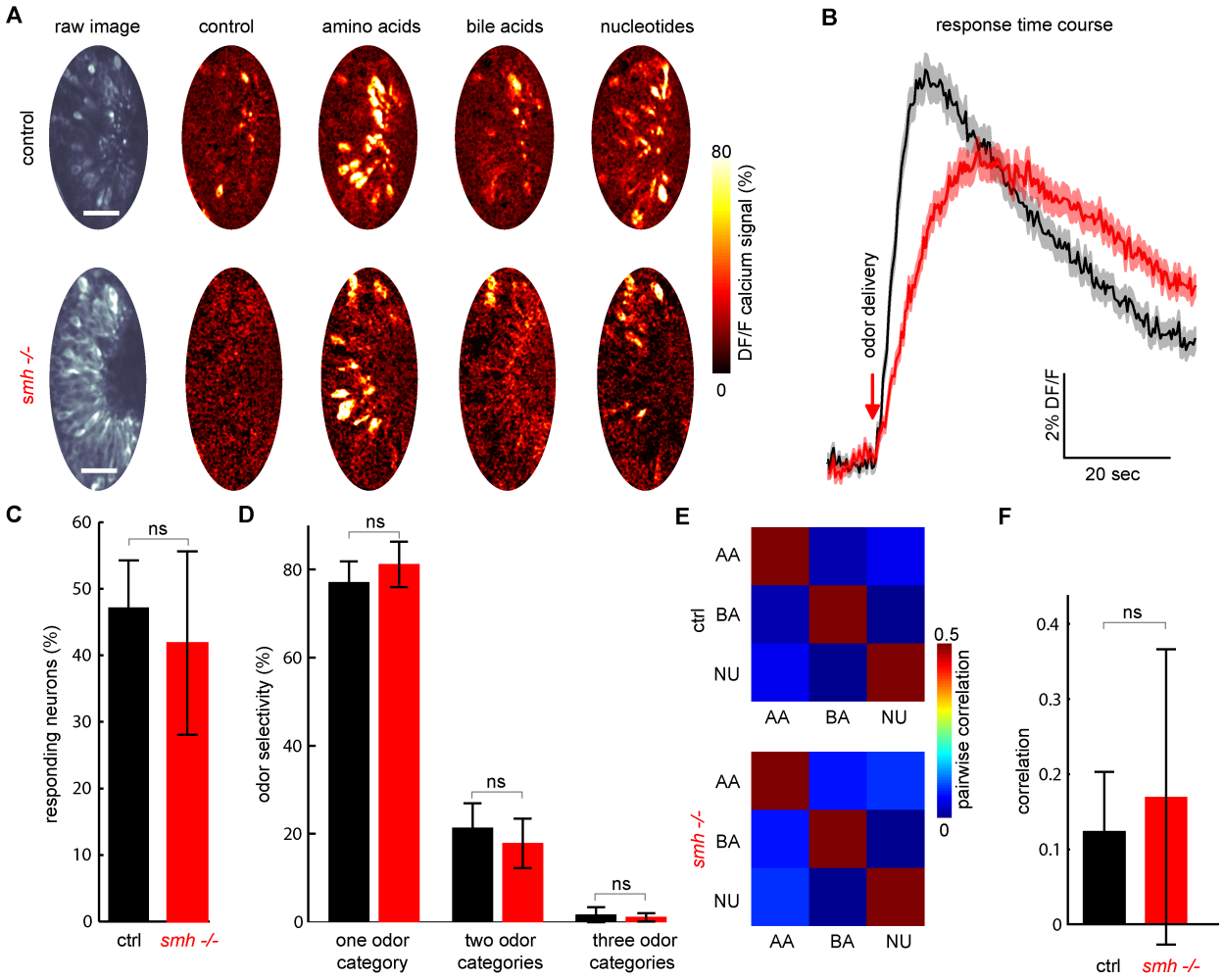

Figure 4: No significant differences were observed in the odor coding of ORNs in *smh-/-* zebrafish, when long (20s) odor pulses are presented with constant flow. (A) Control and *smh-/-* 4 days old zebrafish larvae expressing *HuC:GCamp6s* were exposed to 3 major odor categories: amino acids, bile acids, nucleotides. Representative images show neural responses in the form of relative change in fluorescent intensity (DF/F) in GCamP6s signals of ORNs in control and *smh-/-* larvae. Scale bar is 25µm (B) Average responses of all individual ORNs show slower kinetics of response in *smh-/-* larvae (red), when compared to control (black). (C) The ratio of odor responding ORNs are not significantly different in *smh-/-* versus control animals, in long odor pulses with constant flow. ORNs are considered odor responding if their calcium responses are 2std above the mean activity during baseline. (D) Odor selectivity of responding ORNs to one, two or three of presented odor categories are not significantly different in *smh-/-* larvae, when compared to control animals. (E-F) Odor category selectivity is further quantified by calculating pair wise correlations of odor representations across hundreds of individual ORNs. Average correlation matrices (E) as well as comparison of pairwise odor correlations (F) in individual animals suggest no change in odor selectivity in control vs *smh-/-* larvae. n= 6 (controls) and n=5 (*smh -/-*). Error bars are std. p-value by ranksum test, ns=non significant

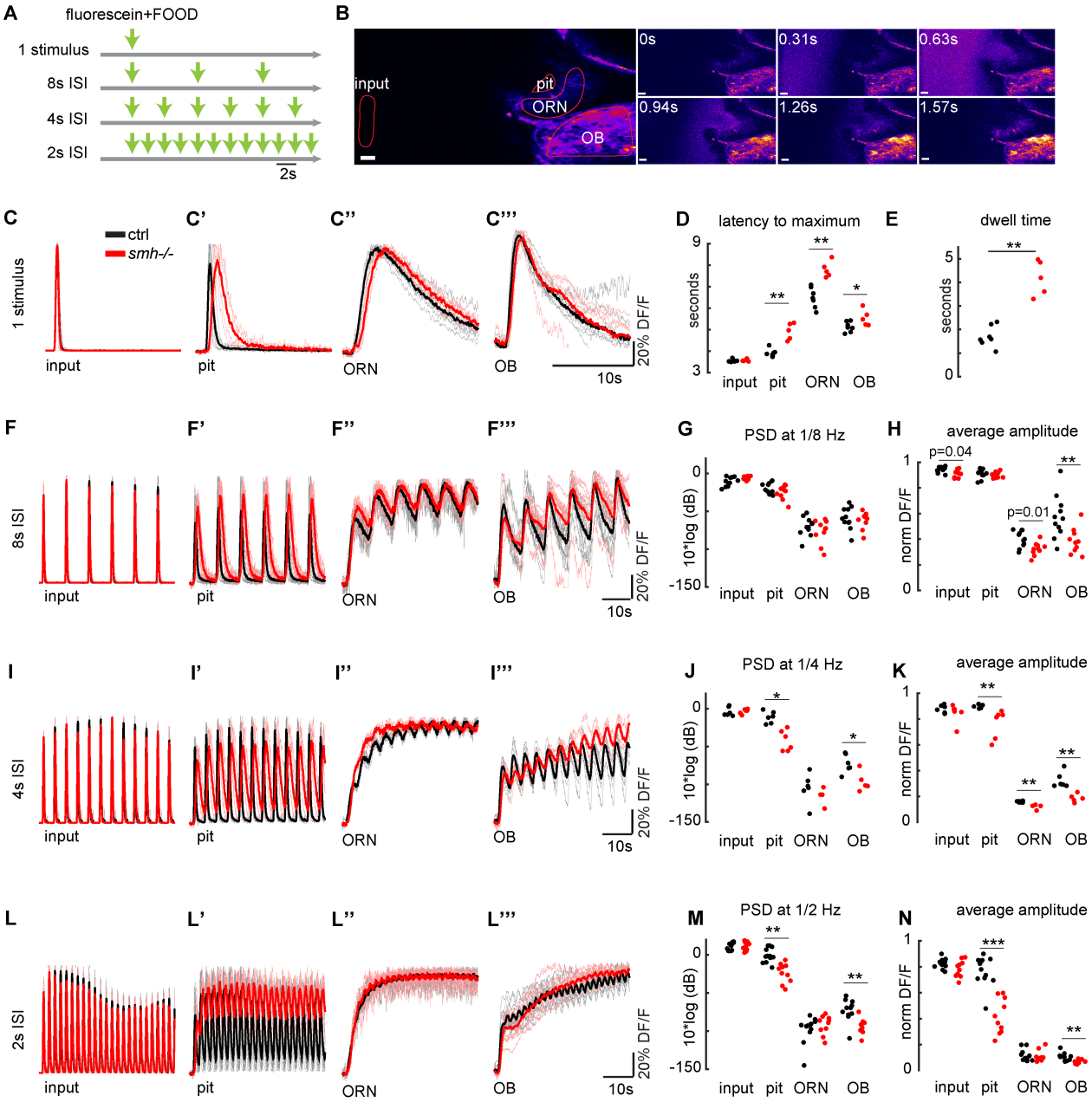

Figure 5: Dynamic sampling of odors via ciliary beating increases the temporal resolution of the olfactory system and enhances the detection of fast changes in odor plumes. (A) Fluorescent-labelled odor pulses of 0.5s are delivered by a pinch valve at various inter-stimulus intervals (ISI) in order to generate odor plumes with increasing frequencies. (B) Montage representing the two photon microscopy images preceding and following the delivery of a single odor pulse. Time in seconds. (C-N) Odor kinetics at the input (C-L) and the nose pit (C'-L') as well as odor responses in ORNs (C''-L'') and OB (C'''-L''') are visualized by two photon microscopy in 4 days old *HuC:Gcamp6* larvae and quantified by the percent change in fluorescence intensity of fluorescein or GCamp6 DF/F in these regions normalized to the maximum for each larvae. Control zebrafish is in black, *smh-/-* zebrafish with no ciliary beating is in red. (C-E) For a single 0.5s odor pulse, odors reach the nose pit with a significant delay (D) and reside longer (C', E) in *smh-/-* zebrafish. As a result ORNs and OB get activated with a delay

(C’’,C’’’,D). (F-N) With decreasing inter-stimulus intervals, while the odor kinetics at the input are similar (F, I, L), the odor signals in the nose pit (F’, I’ ,L’) and odor responses at the level of ORNs (F’’ ,I’’ ,L’’) and OBs (F’’’,I’’’,L’’’) are slower in *smh-/-* zebrafish. The temporal resolution of odor detection is quantified by two different approaches: the power of odor signals (non-normalized DF/F) at the frequency of odor delivery in the nose pit, ORNs and OBs (G, J, M) and the average amplitude of oscillations in normalized odor signals, after the first pulse (H,K,N). Both of these measures confirm that control animals with ciliary beating are significantly better in detecting fast changes in odor dynamic, when compared to *smh-/-* zebrafish with no ciliary beating. Scale bar is 20µm. p-values by ranksum test, ** $p<0.01$, *** $p<0.001$. See also Movie S6 and S7

Supplemental figures and legends

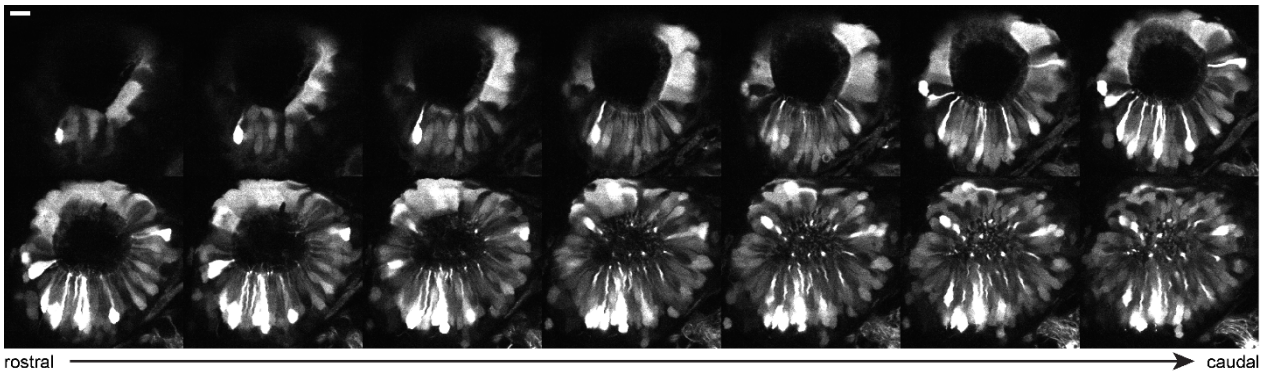

Figure S1: Multiciliated cells bearing motile cilia are located at the periphery of the nose pit above the ORNs. Related to Figure 1. Two photon microscopy optical section of the nose pit in *Foxj1a:GFP* 4 days old larvae at multiple depths from rostral to caudal. Scale bar is 10µm, 2µm spacing between the individual images. Note that the multiciliated cells with motile cilia have a distinct cuboidal shape, which is different from pear shaped ORNs that are also labelled in *Foxj1a:GFP* larvae. Also note that multiciliated cells are arranged in a semi-circle along the nose pit.

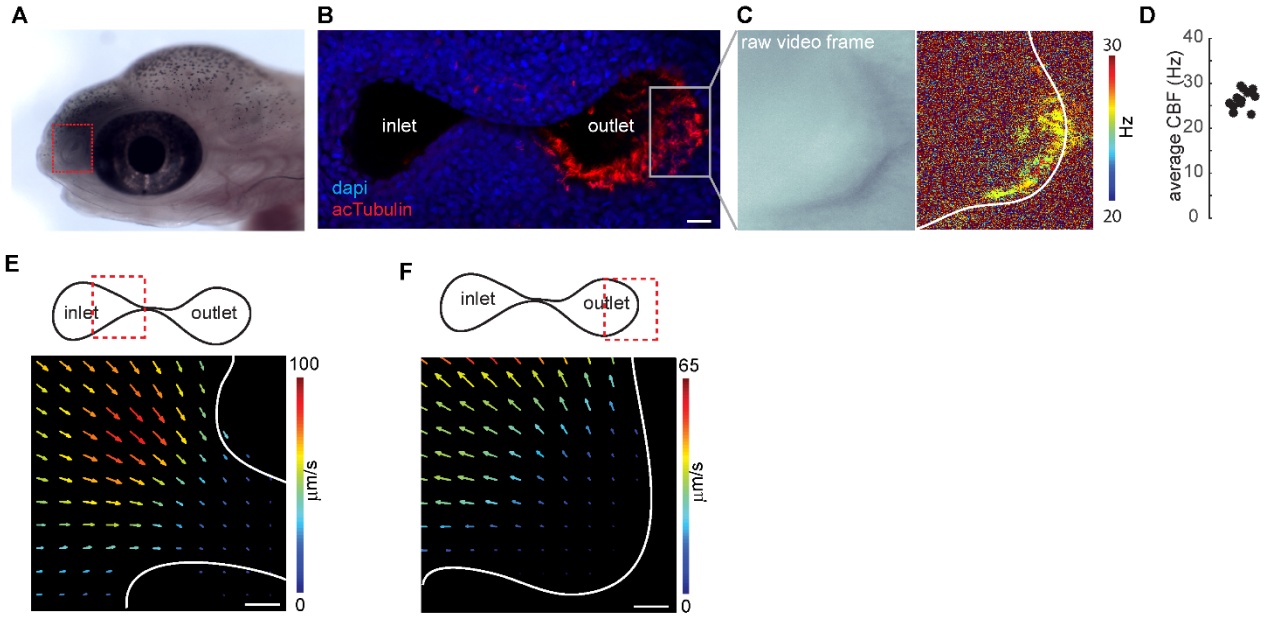

Figure S2: Multiciliated cells in the nose pit of salmon larvae are spatially organized, beat at a distinct frequency and generate a stereotypical flow. Related to Figures 1 and 2. (A) Representative picture of a salmon larvae 4 days post hatching. The nose pit is indicated by a red inlet. (B) Confocal microscopy image of the nose pit, where all cilia are labelled by acetyl tubulin staining (red) and cell nuclei are labelled with DAPI staining (blue). The nose pit is composed of one anterior and one posterior opening connected by one channel. Note the enrichment of acetyl tubulin positive motile cilia at the posterior opening. (C) 100Hz transmission microscopy recordings in the posterior opening of the nose pit (indicated by the inlet on the confocal image) of a representative animal (left) showed that motile cilia beat at frequencies of about 25Hz (right, nose cavity is indicated with a white line). (D) Average ciliary beating frequency from 6 salmon larvae at 2 different locations range from 23.1 to 29.3Hz, with a mean of 26.5 +/-2 Hz. (E-F) Flow fields were calculated by particle image velocimetry in confocal microscopy measurements (19.6 Hz) of fluorescent particles around the nose pits at the inlet (E) and outlet (F). Nose pits are indicated by white lines. Imaging plane viewed from dorsal. Warm colors and large arrows indicate strong flow. Direction of the arrows indicate the direction of the flow. Note that the stereotypical flow fields generated by motile cilia attract water through the inlet to the outlet. Red inlet in the scheme on the top depicts the imaged region. Scale bars are 20µm.

Supplemental Experimental Procedures

Fish maintenance:

The animal facilities and maintenance of the zebrafish, *Danio rerio*, were approved by the NFSA (Norwegian Food Safety Authority). Fishes were kept in 3,5 liter tanks in a Techniplast Zebtech Multilinking system at constant conditions: 28°C, pH 7 and 600µSiemens, at a 14:10 hour light/dark cycle to simulate optimal natural breeding conditions. Fishes received a normal diet of dry food (SDS 100-400, dependent of age) two times/day and Artemia nauplii once a day (Grade0, platinum Label, Argent Laboratories, Redmond, USA). For experiments, the following fish lines were used: *smh* (received from I. Drummond, MGH Boston) [S1], *hspGGFF19B;UAS:GFP, HuC:Gcamp6s* [S2]. *Foxj1a:GFP* transgenic animals were generated in our laboratory upon co-injection of tol2 transposase mRNA and *Foxj1a:GFP* plasmid obtained from X Lin [S3].

smh heterozygous adults were genotyped by PCR followed by restriction analysis with BfaI as described in [S1]. Incross of genotyped heterozygous parents were used in the experiments. Homozygous mutant animals (25% of the clutch) were identified based on their bend body axis. Straight tail larvae coming from the same clutch were used as controls (corresponding to heterozygous and wild-type larvae).

All zebrafish experiments were done in 4 days old zebrafish larvae.

Salmon larvae were obtained from Aquagen AS (Trondheim). Larvae were delivered at 4 days post hatching, corresponding to 544.38 day degrees (10.5 weeks). Experiments were performed on euthanized larvae.

Immunostaining and imaging

PFA-fixed larvae were washed with 0.1%PBS-Tween (0.1%PBST, 3x10min) and permeabilized with acetone (100% acetone, 1h incubation at 20°C). Subsequently, samples were washed with PBS (3x10min) and blocked in 1% BSA/PBS for 1h. Larvae were incubated with acetyl tubulin (6-11B-1, Sigma, 1:1000) overnight at 4C. On the second day samples were washed (0.1%PBST, 4x20min) and subsequently incubated with the secondary antibody (Alexa-labelled GAM568, Life Technology, 1:1000) overnight at 4°C. The third day samples were incubated with 0.1% DAPI in 0.1%PBST, Life Technology, 1hr), washed (0.1%PBST, 4x20min) and transferred to a series of increasing glycerol concentrations (25%, 50% and 75%). Stained larvae were stored in 75% glycerol at 4°C and imaged using a Zeiss confocal microscope with a 10x plan NA 0.3 or 20x plan NA 0.8 objective.

Images of *foxj1a:gfp* larvae was acquired by a two photon microscope (Scientifica) with a 16x water immersion objective (Nikon, NA 0.8, LWD 3.0, plan) and laser of 920 nm wavelength.

Acquired images were processed with ImageJ.

Ciliary beating measurement

High-speed microscopy recordings of motile cilia were conducted with 4 days old larvae paralyzed with α-bungarotoxin (Invitrogen BI601, 1 mg/mL) and then embedded in 2% low melting point agarose prepared in AFW in a Fluorodish (World Precision Instruments). Agarose covering the nostrils was removed to allow free ciliary beating. Olfactory pits of zebrafish larvae were visualized by a Bresser transmitted light microscope using a 63x water immersion objective lens (Zeiss, NA 0.9, plan). High-speed digital recordings were captured with an Allied Vision Manta camera. Frames were acquired and stored by custom made software written in C++, and further analysis was conducted in MATLAB (Mathworks). Videos were acquired at 99-110 frames per second (fps).

Beating cilia interfere with the transmission of light and result in an oscillatory change of light intensity over time. We analyzed the frequency of oscillations for every pixel of the recording using the power spectral density (PSD) estimate via Welch's method (pwelch) of MATLAB. [Pxx(i,k,:),w] = pwelch(Trace,128*4,120,[],Fs,'onesided'). For each pixel, CBF was calculated as the frequency (between 15Hz and half the frequency of acquisition) showing the maximal PSD value. To compute the average CBF of a larvae, PSD estimates of each pixel were averaged and the frequency (between 15Hz and half the frequency of acquisition) showing the maximal PSD value reported as average CBF.

High-speed microscopy recordings of motile cilia of salmon were conducted on euthanized salmon larvae. The head was positioned on a Fluorodish (World Precision Instruments) coated with sylgard and secured by an insect pin.

Light-sheet microscopy

Light sheet microscopy imaging of *hspGGFF19B;UAS:gfp* larvae was used to investigate beating patterns of individual cilia. Olfactory pits of larvae were recorded for 1-2 sec at 700-900 fps. Paralyzed larvae were mounted in agarose in a homemade chamber. Larvae were positioned so that they were directly facing the sheet of laser light from the light sheet microscope. The agarose in front of the olfactory pits was removed. The chamber was filled with AFW so that larvae was completely covered. Microscopy recordings were obtained by a custom-made light-sheet microscope (based on the design described by [S4]) with a 20x water immersion objective (Olympus, NA 1.00, plan) and a laser of 488 nm wavelength (Cobolt). Images were acquired by the Zebrascope software in LabView [S4] and analyzed in ImageJ/Fiji and MATLAB. To obtain a kymogram, the function improfile of MATLAB was used. In order to measure the velocity of cilia during the power stroke, the tips of cilia were tracked manually on ImageJ/Fiji. The velocity was calculated as distance/time.

Flow fields

Paralyzed 4 days old larvae were embedded in 2% low melting point agarose prepared in AFW in a Fluorodish. Agarose was removed around the head to avoid any disturbance of the flow. 0.16um fluorescent particles (Spherotech, 1:200 dilution) were added to the AFW. Recordings of flow fields from salmon were done on euthanized salmon larvae, positioned on a Fluorodish coated with sylgard and secured by an insect pin.

Time lapse images were acquired on a confocal microscopy (20x water immersion, NA 1) at either 512x512 pixel with 465ms/frame (big field of view) or 128x128 pixel, 3x zoom with 51.2ms/frame (small field of view). Particle images were processed in DaVis 8.2 (LaVision GmbH, Gottingen, Germany). All recordings included 1200 image frames. Multiple interrogation windows with decreasing size were used for vector calculations. Interrogation size from 128x128 to 48x48 pixels with 50% and 2 passes were used for flow recordings with 512x512 pixels resolution. Interrogation size from 64x64 to 12x12 pixels with 50% and 2 passes were used for flow recordings with 128x128 pixels resolution. During processing, masking was applied to fish body. Smoothing and median filter were used to smooth vectors and eliminate the neighboring bad vectors, respectively.

Residence time was obtained by the following equation: (length of particle path)/ average velocity. Average velocity is average of maximum velocities of inflow and outflow. Length of particle path (38.48um) was determined upon fitting a curve (20 um above the surface of pit due to cilia) as path of flow particle in the pit by using the dimensions of pit.

Calcium imaging

4 days old control and *smh-/- HuC:GCamp6* zebrafish larvae were paralyzed and mounted in 2% low melting point agarose prepared in AFW. The agarose surrounding the nostril was removed to allow odors to reach the epithelium. All experiments were done on a 2photon microscope (Scientifica) with a 16x water immersion objective (Nikon, NA 0.8, LWD 3.0, plan). A mode-locked Ti:Sapphire laser (MaiTai Spectra-Physics) tuned to 920 nm was used for excitation. Either single plane or volumetric recording (6 planes with a Piezo) were obtained. Acquisition rate were 31.56Hz for a single plane of 512x500 pixels or 2.99Hz for a volume of 1536x900 pixels x 6 planes. The change of fluorescence was estimated as the relative change of fluorescence over time by dF/F, $F-F_{baseline}/F_{baseline}$. $F_{baseline}$ was the average value of the frames before the stimulus delivery. Data analysis was done with MATLAB as described in subsequent section.

Preparation of odors

For food odor, 1g of dry food (SDS 100) was incubated in 50ml AFW for 1h, the mixture was then filtered through a filter paper and diluted 1:50. Fluorescein (10-4M) was added to the solution. All odor aliquots were prepared from stock solutions (Sigma Aldrich, 10mM) dissolved in AFW and stored in a -20°C freezer. The following fresh odor mixtures were prepared weekly at 0.1mM. Amino Acid-mix: Alanine, Phenylalanine, Aspartic acid, Arginine, Methionine, Asparagine, Histidine. Bile-mixture: IMP and AMP. Nucleotides-mix : TCA + TDCA

Olfactory stimulation and data analysis

Odor delivery in stagnant environment with microinjector: odors (50x concentrated) were delivered by a glass capillary pulled with a laser puller (Sutter) connected to a microinjector (Femtojet, Eppendorf). A single injection was manually delivered using the following settings: 70Pi, 0.2s, 5 back pressure. The capillary was positioned around 200µm away from the nostril. 3 regions of interest (ROI) were manually drawn in the pit, surrounding the

ORN and OB. DF/F was smoothened using a window of 5 frames. 2 independent odor deliveries were done for each larvae and results were averaged.

Odor coding and selectivity in constant flow: odors were delivered through a constant flow (2ml/min) using an Arduino Due -controlled, pneumatically actuated HPLC injection valve (Valco Instruments). Odor applications were delivered in a randomized order. Volumetric images were first aligned using a custom-written algorithm adapted from [S5]. Somata from individual neurons were segmented into distinct ROIs using a custom written MATLAB algorithm detecting ROIs manually. Fluorescence time courses for each neuron were averaged across three stimulus trials, and baseline fluorescence before stimulus onset was subtracted. Neurons are considered responding if the odor responses exceed 2 std deviation above the baseline period for at least one of the odors. Odor selectivity was calculated among neurons that are responding to at least one of the presented odors. Correlations are calculated as Pearson's correlations of the odor response vectors. Odor response vectors are calculated as the responses of all ORNs during the first 50 seconds of odor response.

Temporal resolution of fast changing odor plumes: short (0.5s) odor pulses were delivered through a constant flow of AFW (2ml/min) using an Arduino Due-controlled pinch valve. 4 ROI were manually drawn at the exit of delivery tubing (input), in the pit, surrounding the ORNs and OB neurons. DF/F was smoothened using a window of 5 frames. Data for each ROI were normalized to maximum so that maximal DF/F was set to 1. 2 independent odor deliveries were done for each larvae and averaged. Time to maximal amplitude was calculated as the time when the DF/F is maximal after the activation of the pinch valve. Amplitude of oscillation was calculated on normalized DF/F as follows: for each odor stimulus from the second stimulus to the end (6 stimuli for 8s ISI, 30 stimuli for 4s ISI, 40 stimuli for 2s ISI), the minimal and maximal DF/F value was determined and the difference reported as the amplitude. This amplitude was then averaged for all odor pulses. Power spectral density was calculated on non normalized DF/F data using the periodogram Welch's method (pwelch) of MATLAB.

Statistics:

Statistical analysis was done using MATLAB. Wilcoxon ranksum test was used for non paired analysis and Wilcoxon signed rank test for paired analysis. $P<0.05$ was considered as statistically significant.

Supplemental References

S1 Panizzi, J.R., Becker-Heck, A., Castleman, V.H., Al-Mutairi, D.A., Liu, Y., Loges, N.T., Pathak, N., Austin-Tse, C., Sheridan, E., Schmidts, M., et al. (2012). CCDC103 mutations cause primary ciliary dyskinesia by disrupting assembly of ciliary dynein arms. Nature genetics *44*, 714-719.

S2. Quirin, S., Vladimirov, N., Yang, C.T., Peterka, D.S., Yuste, R., and Ahrens, M.B. (2016). Calcium imaging of neural circuits with extended depth-of-field light-sheet microscopy. Opt Lett *41*, 855-858.

S3. Caron, A., Xu, X., and Lin, X. (2012). Wnt/beta-catenin signaling directly regulates Foxj1 expression and ciliogenesis in zebrafish Kupffer's vesicle. Development *139*, 514-524.

S4. Vladimirov, N., Mu, Y., Kawashima, T., Bennett, D.V., Yang, C.T., Looger, L.L., Keller, P.J., Freeman, J., and Ahrens, M.B. (2014). Light-sheet functional imaging in fictively behaving zebrafish. Nat Methods *11*, 883-884.

S5 Bergen, J.R., Anandan, P., Hanna, K.J., and Hingorani, R. (1992). Hierarchical model-based motion estimation. In Computer Vision — ECCV'92: Second European Conference on Computer Vision Santa Margherita Ligure, Italy, May 19–22, 1992 Proceedings, G. Sandini, ed. (Berlin, Heidelberg: Springer Berlin Heidelberg), pp. 237-252.